Open Access

Carrier Redistribution Between Two Kinds of Localized States in the InGaN/GaN Quantum Wells Studied by Photoluminescence

Yao Xing[1,2] , Degang Zhao[1,3*], Desheng Jiang[1], Zongshun Liu[1], Jianjun Zhu[1,3], Ping Chen[1], Jing Yang[1], Feng Liang[1], Shuangtao Liu[1] and Liqun Zhang[4]

Abstract

The InGaN/GaN multi-quantum wells (MQWs) are prepared at the same condition by metal-organic chemical vapor deposition (MOCVD) except the thickness of cap layers additionally grown on each InGaN well layer. The photoluminescence (PL) intensity of the thin cap layer sample is much stronger than that of thicker cap layer sample. Interestingly, the thick cap layer sample has two photoluminescence peaks under high excitation power, and the PL peak energy-temperature curves show an anomalous transition from reversed V-shaped to regular S-shaped with increasing excitation power. Meanwhile, it exhibits a poorer thermal stability of thick cap layer sample under higher excitation power than that under lower excitation power. Such an untypical phenomenon is attributed to carrier redistribution between the two kinds of localized states which is induced by the inhomogeneous distribution of indium composition in thick cap layer sample. Furthermore, the luminescence of deep localized states has a better thermal stability, and the luminescence of shallow localized states has a poor thermal stability. In fact, such a severer inhomogeneous indium distribution may be caused by the degradation of subsequent epitaxial growth of InGaN/GaN MQWs region due to longer low-temperature GaN cap layer growth time.

Keywords: Semiconductor materials, InGaN/GaN multiple quantum wells, Photoluminescence, Carrier localization

Introduction

InGaN/GaN multi-quantum well (MQW) structure has received great attention due to its wide use in light-emitting diodes (LEDs) and laser diodes (LDs) [1–6]. Although the high threading dislocation density and reduction of wave function overlap caused by spontaneous and piezoelectric polarization of InGaN/GaN MQWs, their luminance efficiency is still surprisingly high [7–10]. One of the main reasons is that the localization of excitons in potential minima due to fluctuations of indium content leads to the formation of quantum-dot-like states in InGaN/GaN quantum wells [11]. However, it remains ambiguous how the roles localization states play on the luminescence mechanism. Several studies have reported the effect of InGaN composition fluctuations on radiative and Auger recombinations [12–14]. Theoretical simulations of atomistic tight-binding used by Jones found that the localization increases both radiative and Auger recombination rates, but Auger recombination rate increases by one order of magnitude higher than radiative one [15]. Experimentally, carrier localization leads to the relaxation of the k-selection rule in the Auger recombination process, and thus strongly enhances the Auger recombination process in polar InGaN/GaN QWs under high optical excitation [16]. It is well known that the temperature-dependent S-shaped behavior of luminescence peak energy is a fingerprint of carrier localization. Many models, such as localized state ensemble (LSE) model, are proposed to

* Correspondence: dgzhao@red.semi.ac.cn
[1]State Key Laboratory of Integrated Optoelectronics, Institute of Semiconductors, Chinese Academy of Science, Beijing 100083, China
[3]Center of Materials Science and Optoelectronics Engineering, University of Chinese Academy of Sciences, Beijing 100049, China
Full list of author information is available at the end of the article

explain the carrier localization and thermal redistribution behavior, showing that the variation of luminescence peak energy with temperature can be influenced by unique carrier redistribution process under different excitation levels [17–21]. Generally, the manufactured devices like laser diodes are always operating with a higher injected carrier density [22]. In this case, the photoluminescence spectra of localized states may exhibit a unique behavior at different excitation level associated with the uniformity of localized states. Further studies are therefore necessary to understand the effect of alloy fluctuations on InGaN devices.

In this work, two typical samples with different thickness of GaN cap layers which are additionally grown on each InGaN well layer are prepared by metal-organic chemical vapor deposition system (MOCVD). The properties of MQWs are characterized in detail by high-resolution X-ray diffraction (HRXRD), temperature-dependent photoluminescence (TDPL), and power-dependent photoluminescence (PDPL) measurements. It is found that the thick cap layer sample shows an anomalous peak at higher energy side under high optical excitation power. This implies a co-existence of two different kinds of localized states. Meanwhile, the PL intensity decays faster at low temperatures when the excitation power is increasing higher. Hence, we can assume that the photoluminescence of deep localized states has a better thermal stability, and the photoluminescence of shallow localized states has a poor thermal stability.

Methods
Materials
The InGaN/GaN MQW samples with different cap layer thickness grown on c-plane sapphire substrate by an AIXTRON 3 × 2 in close-coupled showerhead reactor are studied. Trimethylgallium (TMGa), trimethylindium (TMIn), and ammonia (NH_3) were used for the epitaxial growth as Ga, In, and N source precursors, respectively, in which H_2 and N_2 were the carrier gas of the GaN and InGaN growth, respectively. MQW is consisted of two periods of InGaN/GaN QWs. During the growth of each well layer, the TMIn flow rate was kept constant. Then a GaN cap layer was grown at the same temperature as well layer, i.e., 710 °C. Afterwards, the temperature was ramped up to 830 °C, and stay several seconds, and then the barrier layer was grown at 830 °C. Both samples A and B are grown under the same conditions except the GaN cap layer growth time, i.e., it is 30 s for sample A and 200 s for sample B. The schematic diagram of structure and growth parameters of two InGaN/GaN MQWs A and B are shown in Fig. 1.

Characterization
To determine the average indium content, period thickness, and material quality of two InGaN/GaN MQWs,
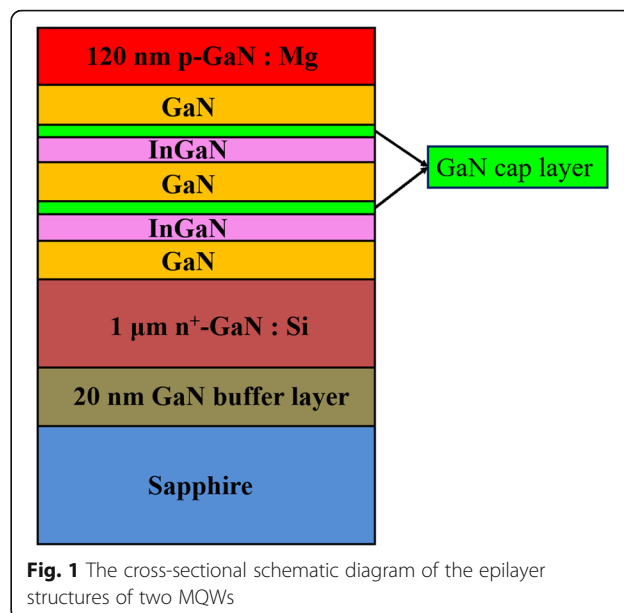

Fig. 1 The cross-sectional schematic diagram of the epilayer structures of two MQWs

high-resolution x-ray diffraction (HRXRD) measurement is performed with Rigaku Ultima IV with Cu-Ka radiation (λ = 1.54 Å) that operated at 40 kV and 30 mA. For temperature-dependent photoluminescence (TDPL) and excitation power-dependent PL (PDPL) measurements, a 405 nm laser was used as an excitation light source with spot size of 0.5 mm^2, and the excitation power varied from 0.01 to 50 mW. The samples were mounted in a closed-cycle He cryostat and the temperature was controlled from 10 to 300 K.

Results and Discussions
To investigate the structural properties of two samples A and B, the ω-2θ symmetrical (0002) scans have been carried out, as shown in Fig. 2a. The substrate peak originates from GaN (002) plane, and satellite peaks come from MQWs. Satellite peaks up to the fourth order can be clearly observed in all two samples, indicating a good layer periodicity. In addition, the average indium composition and periodic thickness can be obtained by fitting the measured curves, as shown in Table 1. It can be seen that as the thickness of cap layer increases, the GaN barrier thickness and the thickness and indium composition of InGaN well layers increase slightly. Actually, because the growth rate of cap layer is as small as 0.006 nm/s and the growth temperature is as low as 710 K, the change of barrier thickness is relatively small. However, noting that the growth of additional GaN cap layers may have influences not only on the barrier layer thickness but also on the diffusion, evaporation, and redistribution of In atoms in the InGaN well layers, as will be discussed in detail later.
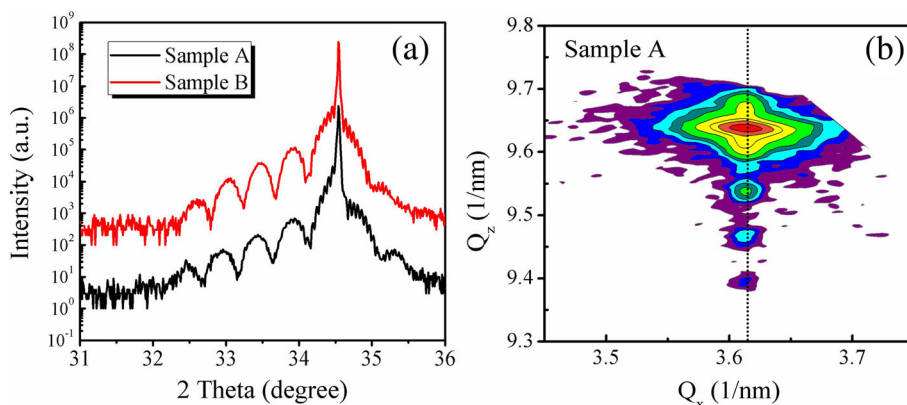
Fig. 2 Omega-2theta scans and reciprocal space mapping of both samples are performed by HRXRD. **a** HRXRD Omega-2theta curves on GaN (0002) plane for samples A and B. **b** Reciprocal space mapping (RSM) for the GaN (10–15) diffraction of sample A

Meanwhile, to examine the strain state of GaN QB and InGaN QW layers, reciprocal space mapping (RSM) in the vicinity of the GaN (10–15) plane is performed. The result of sample A is shown in Fig. 2b (The RSM figure of B is similar, but not shown here). We can observe that for sample A, the satellite peaks of MQW and GaN peak align well on the same vertical line, indicating that the MQWs of both samples are fully strained without any relaxation [23].
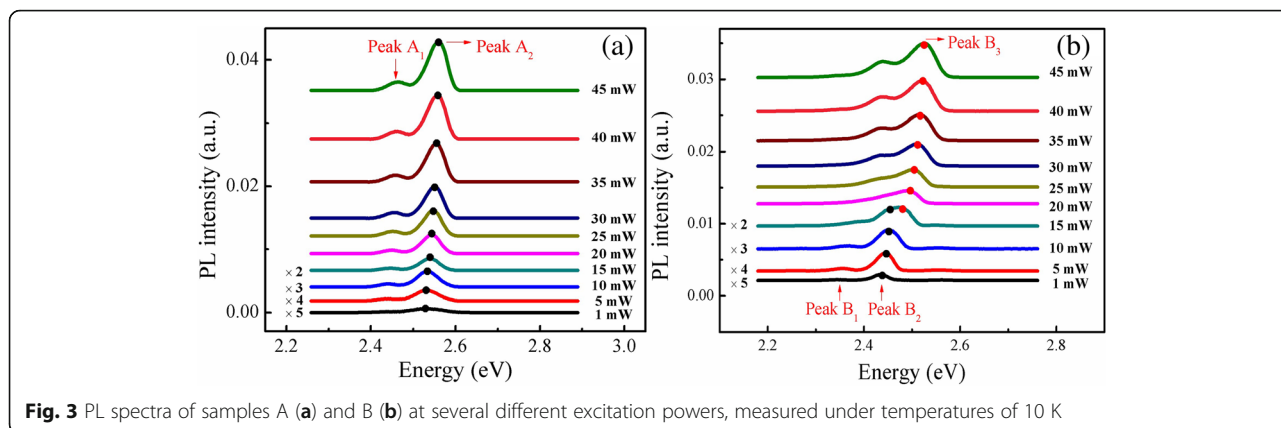
Figure 3 shows the PDPL measurements for two samples at 10 K. It is interesting to find that the two samples exhibit quite different behaviors. For sample A, there is a small peak located at lower energy side (peak A_1) of dominant peak A_2. It is confirmed that peak A_1 is phonon replica which is 92 meV away from the main peak A_2. The phonon replica of B_2 also appears in sample B and is called as peak B_1. On the other side, in Fig. 3b, it can be observed that there is only one dominant luminesce peak B_2 with the excitation power lower than 5 mW. However, when the excitation power is higher than 10 mW, another peak B_3 abnormally appears at higher energy side of B_2, and peak B_3 gradually becomes the dominant emission peak instead of peak B_2 when the excitation power increases further. Here, we can assume that the majority of the optical excited carriers first got trapped in the first type of electronic states (e.g., localized states created by the local In-rich clusters), and then radiatively recombine, producing luminescence peak A_2 and B_2. [24].

Table 1 Structural parameters of InGaN/GaN MQWs of samples A and B determined by HRXRD

Samples	Cap layer growth time (s)	Period thickness (nm)	Barrier thickness (nm)	Well thickness (nm)	In content in InGaN
A	30	19.10	14.85	4.25	10.0%
B	200	19.95	15.50	4.45	10.3%

To examine the behavior of anomalous peak B_3 of sample B further, we have performed the TDPL measurements under different excitation powers shown in Fig. 4, in which Fig. 4a and b are the PL spectra obtained under excitation power of 5 mW and 40 mW, respectively. Note that the two-peak phenomenon of the emission spectra in Fig. 4b was clearly seen at temperatures below 200 K and became blurred toward 300 K. Summarizing the emission spectra behavior, one can see that the transition from the low energy emission peak to the high energy emission peak occurs in a narrow range of excitation power and has a "switching" character. Outside the narrow transition region, single low energy (B_2) or high energy (B_3) emission peak dominates at low and high excitation powers, respectively.

Additionally, a closer inspection of the variation of dominant emission peak energy with temperature of both samples, we can find something unique. As shown in Fig. 5a, when the excitation power increases from 5 to 40 mW for sample A, the variation of PL peak energy with increasing temperature (called E-T curve below) shows "reversed V shape" curves, which is different from the regular "S" shape. The reversed V shape is almost unchanged with increasing excitation power except an overall blue shift of the peak energy. The reversed "V"-shaped temperature dependence is explained as a joint action of carrier filling effect at luminesce centers and bandgap shrinkage effect accompanied with increasing temperature [25, 26]. On the other hand, as shown in Fig. 5b, the E-T curves for sample B under the excitation power lower than 5 mW show a reversed V shape. This situation is similar to sample A. However, when the excitation power gradually increases to 40 mW, a first redshift appears at lower temperature range, and the E-T curves have a regular S shape. Apparently, this phenomenon contradicts the expectation that when the excitation power is large enough, the localization effect will completely disappear, and the temperature

Fig. 3 PL spectra of samples A (**a**) and B (**b**) at several different excitation powers, measured under temperatures of 10 K

behavior of the peak energy will closely follow the Varshni law [27].

Thus, to quantitatively explain the observed anomalous excited optical power dependence of luminescence of localized states, the LSE luminescence model was employed to fit the E-T curves, which is proposed by Q. Li et al. This model can be used in all temperature ranges, and it can not only fit the "S" shape E-T curves but also the "V" or reversed "V" shapes. In addition, it was also proved that LSE model can be reduced to Eliseev et al.'s band-tail model at high temperatures [24, 25]. In this model, the peak energy as a function of temperature can be described as [18–21]:
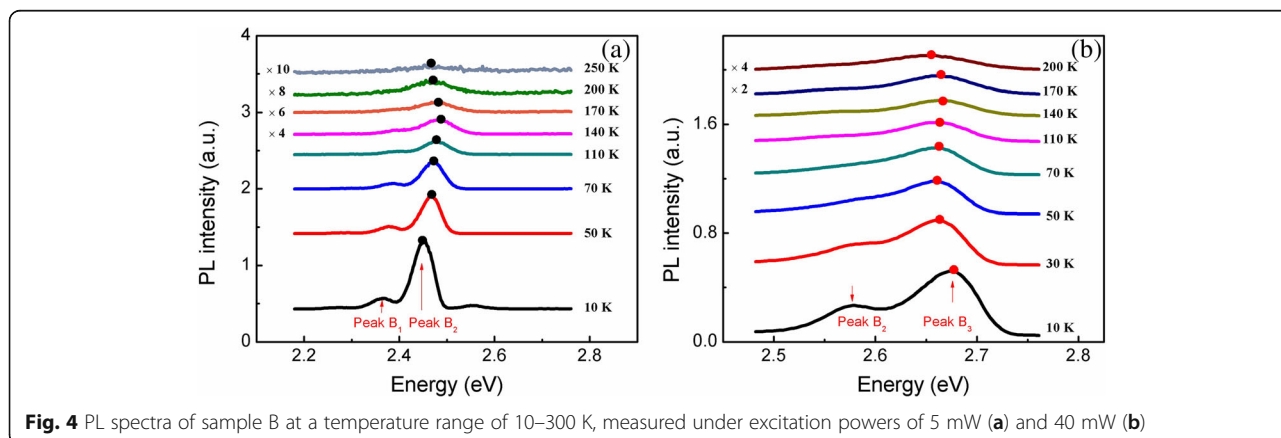
$$E(T) = \left(E_0 - \frac{\alpha T^2}{\theta + T} \right) - x k_B T \tag{1}$$
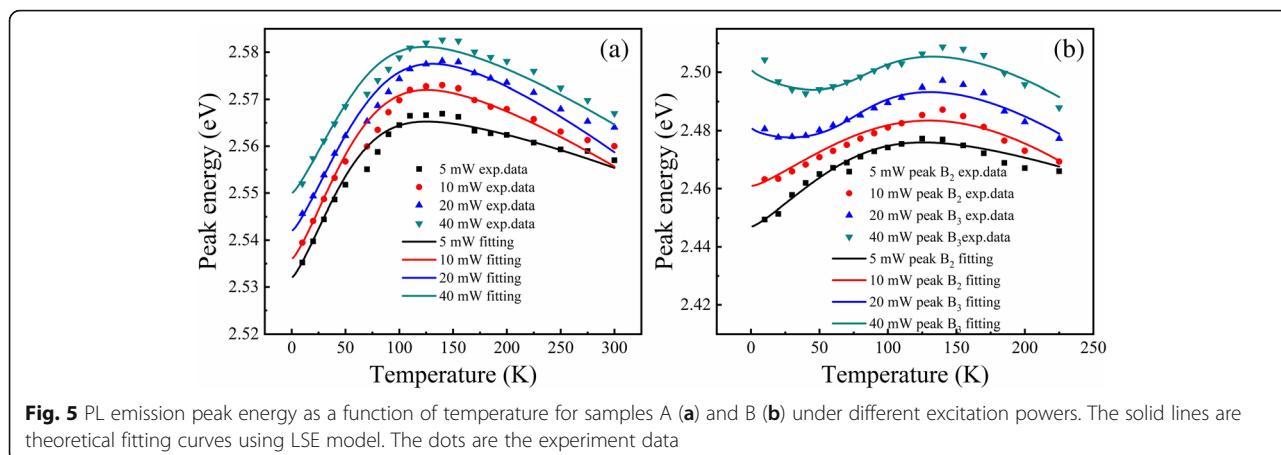
where θ is the Debye temperature of the specific material and a is the Varshni parameter, k_B is the Boltzmann constant, and x can be numerically solved by the following transcendental equation [18–21]:

$$x e^x = \left[\left(\frac{\sigma}{k_B T} \right)^2 - x \right] \left(\frac{\tau_r}{\tau_{tr}} \right) e^{(E_0 - E_a / k_B T)} \tag{2}$$

where σ is the standard deviation of distribution of the localized states. In other words, it means the width of Gaussian-type state density distribution. τ_r and τ_{tr} represent the radiative recombination and escape lifetime of the localized carrier, and thus τ_r / τ_{tr} implies the portion of carriers which recombines nonradiatively. E_0 is the central energy of the localized centers, and E_a gives a "marking" level below which all localized states are occupied by carriers at 0 K which is just like the quasi-Fermi level in the Fermi-Dirac distribution. It is obvious that E_0 and E_a together are related to the origin of luminescence localized centers [17].

The obtained fitting parameters of both samples are shown in Table 2. For sample A, the central energy E_0 and E_a changes to 19 meV and 18 meV from 5 to 40 mW, respectively. It is noticed that the E_0-E_a and σ is almost unchanged. It is because that as the excited power increases, more and more carriers will be excited. First, the strong piezoelectric field of InGaN wells will be screened by the photogenerated carriers, leading to an increase of central energy E_0. Second, more and more carriers will occupy higher electronic states according to the filling effect, which results in the increase of quasi-Fermi level of localized carriers E_a. Therefore, E_0-E_a represents the joint

Fig. 4 PL spectra of sample B at a temperature range of 10–300 K, measured under excitation powers of 5 mW (**a**) and 40 mW (**b**)

Fig. 5 PL emission peak energy as a function of temperature for samples A (**a**) and B (**b**) under different excitation powers. The solid lines are theoretical fitting curves using LSE model. The dots are the experiment data

action of polarization screening effect and carrier filling effect, and thus an overall blueshift in peak position for sample A is observed. Unlike sample A, for sample B, from 5 to 40 mW, there are bigger increases of E_0 and E_a, 73 meV and 57 meV, respectively. E_0-E_a increase by 16 meV, τ_r/τ_{tr} changes by several orders of magnitude, and σ decreases a little. Such changes are so big that we have to assume that the origin of luminescence centers is different at different excitation powers of 5 mW and 40 mW.
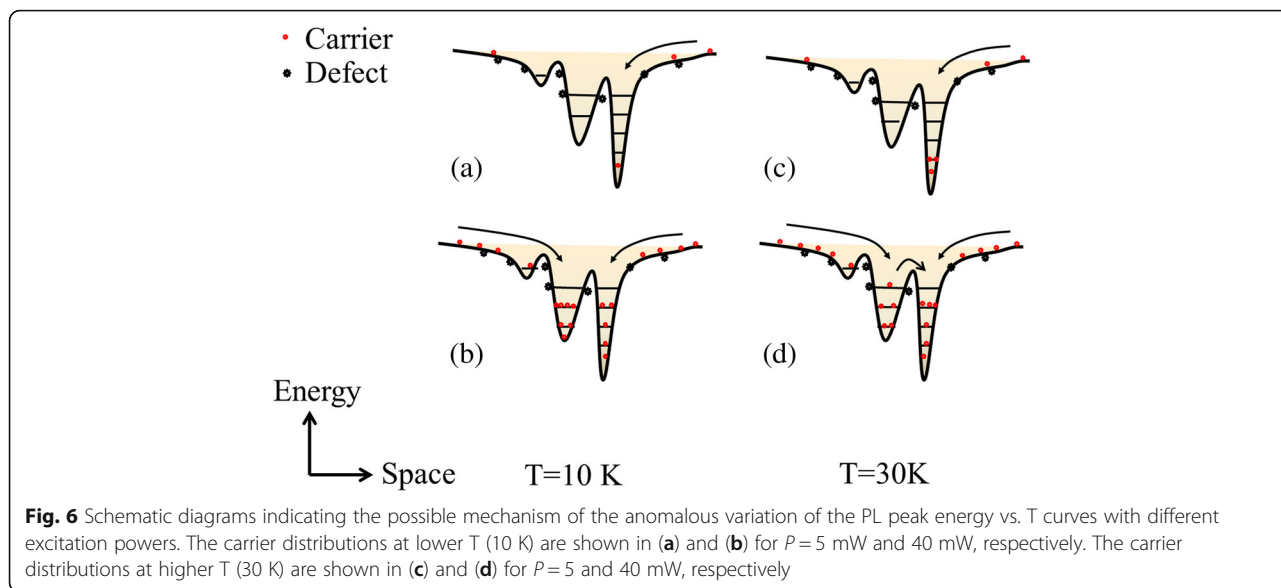
Therefore, it is suggested that for sample B, there are two kinds of localization states, distributing at two different energy depths in the well layers due to the inhomogeneous distribution of indium composition, i.e., with higher indium composition (deep localization states) and lower indium composition (shallow localization states). In addition, to explain the above phenomenon of sample B, the schematic diagrams indicating the possible mechanism of the carrier redistribution between two kinds of localized states are plotted in Fig. 6. At 10 K, under lower excitation power such as 5 mW, shown in Fig. 6a, the majority of the optical excited carriers first get trapped in the first type of electronic states (deep localized states) and thus the lower energy peak dominates, while at 40 mW, shown in Fig. 6b, more and more photogenerated carriers will occupy the

higher energy level, and then the shallow localized states with the higher energy state density are also filled, and thus the higher energy peak dominates gradually with the increase of excited power. Therefore, E_0 and E_a increase a lot, and τ_r/τ_{tr} increase by several orders which imply the escape ability of carriers out of localized states. As the temperature increases to 30 K, at 5 mW, as shown in Fig. 6c, the photogenerated carriers with a certain amount of thermal energy are mainly used to filling the deeper localized states, resulting in a first blueshift of E-T curves; however, in Fig. 6d, when it comes to 40 mW, based on the assumption that shallow localized states have more capacity than the deep localized states, the majority of the photogenerated carriers stay in shallow localized states, and it will be able to transfer to deep localized states which has a strong ability to bind carriers. Therefore, the E-T curves redshift. In other words, the appearance abnormal changes of E-T curves are concerned with multiple kinds of localization states due to the inhomogeneous indium distribution in InGaN well layers of sample B. And such compositional fluctuations are supposed to be mainly due to the random alloy fluctuations on an atomic scale [28].

Furthermore, the appearance of high energy emission peak under high excitation power of sample B also leads to an anomalous variation of the PL integrated intensity. In Fig. 7, the integrated intensity vs. temperature curves of samples A and B measured at excitation powers of 5 mW and 20 mW are plotted, respectively. First, note that the thermal quenching of sample B is obviously quicker than that of sample A. Generally, the luminescence thermal quenching of the InGaN MQWs is dominated by the nonradiative recombination processes which can be described by Arrhenius equation. Therefore, the quick thermal quenching implies a poor thermal stability of sample B. Furthermore, when the excitation power is high enough, the impact of nonradiative recombination centers at relatively low temperatures will not be so much

**Table 2** Fitting parameter in the LSE model for two samples

Samples	Excited power (mW)	E_0 (eV)	E_a (eV)	E_0-E_a (meV)	$\frac{\tau_r}{\tau_{tr}}$	σ (meV)
Sample A	5	2.57	2.532	38	0.004	14
	10	2.579	2.538	41	0.004	14
	20	2.585	2.545	40	0.004	15
	40	2.589	2.55	39	0.003	15
Sample B	5	2.486	2.447	39	0.003	24
	10	2.516	2.461	55	0.009	30
	20	2.541	2.481	60	1.99	19
	40	2.559	2.504	55	15.01	20

Xing *et al. Nanoscale Research Letters* (2019) 14:88

Page 6 of 8

Fig. 6 Schematic diagrams indicating the possible mechanism of the anomalous variation of the PL peak energy vs. T curves with different excitation powers. The carrier distributions at lower T (10 K) are shown in (**a**) and (**b**) for P = 5 mW and 40 mW, respectively. The carrier distributions at higher T (30 K) are shown in (**c**) and (**d**) for P = 5 and 40 mW, respectively

significant, because the nonradiative recombination centers are easily saturated by excess carriers [27]. This can perfectly explain the slower variation of PL integrated intensity vs. 1/T curves with the increase of excitation power of sample A. However, it is quite interesting for sample B that the normalized integrated intensity under excitation power of 5 mW is even higher than that under 20 mW when the temperature is lower than 125 K, and it turns to be opposite at temperatures higher than 125 K. As mentioned before, it is assumed that only one lower energy emission peak which is originated from deep localized states is dominant at 5 mW, while another higher one originated from shallow localized states becomes dominant at 20 mW. Therefore, it is concluded that the deep

Fig. 7 The integrated intensity extracted from PL spectra of both samples at a temperature range of 10–300 K, measured under excitation powers of 5 mW and 20 mW

localized luminescence centers have better luminescence efficiency than shallow luminescence centers. This agrees well with the previous research result related to the localized states [28]. Therefore, it can also be proved, to some extent, that there are two kinds of localized states excited at 20 mW for sample B.

Based on all these analyses, we demonstrate that peak B_3 originates from the localization states with lower potential related to the inhomogeneous distribution of indium composition of sample B. It agrees well with the experimental results of the higher emission energy peak B_3 and the reduction of IQE of sample B at low temperatures under higher excitation power. Actually, in the growth process of QWs, considering the pulling effects, indium atoms are prone to accumulate at the top of InGaN QW layer and form an extra layer known as indium floating layer [29]. Thicker GaN cap layer growth at low temperature is detrimental to the evaporation of these indium floating atoms. Consequently, In atoms may incorporate into GaN cap layer and barrier layer after the QW growth [30]. Naturally, this behavior will result in an increase of well layer thickness, and thus the QCSE is enhanced. The higher strain and the stronger piezoelectric field in the active QW would induce more localized relaxation and, thus, deeper localized potentials and higher barriers. Meanwhile, more dislocations and defects are introduced into the subsequent growth of GaN barrier layer. Generally, there is large tensile stress near dislocations, and indium atoms may tend to accumulate near the dislocations and distribute inhomogeneously. [31, 32] Therefore, in the growth of InGaN well layer, there are more indium-rich and indium-poor areas associated with the increasing dislocation density. It means that the scale of indium fluctuations will become

Xing *et al. Nanoscale Research Letters*   (2019) 14:88

Page 7 of 8
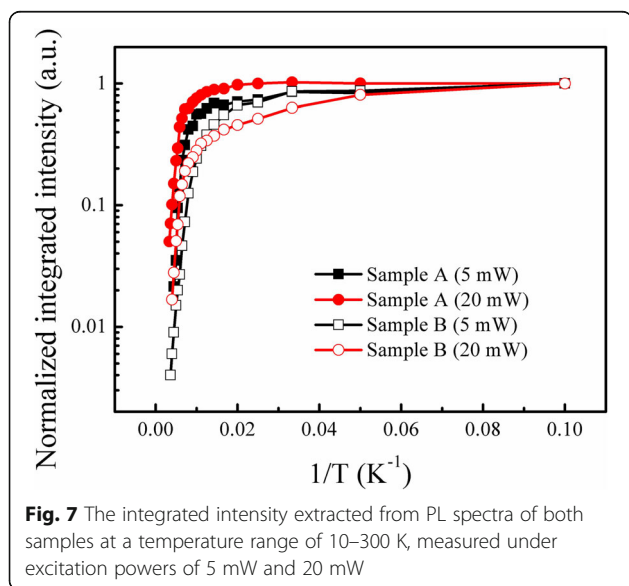
larger as the capping layer thickness increases. In our experiments, it shows that two different kinds of localization states are introduced into sample B with thicker cap layer, and the PL peak of higher emission energy is activated under higher excitation power. On the other hand, the photogenerated carrier stay at deep localized states can screen away the defects and thus has a better thermal stability, while the photogenerated carrier stay at shallow localized states will be captured by the defect-related nonradiative recombination once they can overcome the relatively lower barrier height.

Conclusions

In summary, the InGaN/GaN multi-quantum well (MQW) samples with different thickness of GaN cap layers additionally grown on the InGaN well layers are prepared by metal-organic chemical vapor deposition system (MOCVD). Their structural and optical properties are investigated by HRXRD, TDPL, and PDPL measurements and analyzed. PDPL results show that an additional high-emission energy peak is excited at higher excitation power only for sample B which is grown with thick cap layers. Meanwhile, TDPL results measured at different excitation powers for sample B reveal that the E-T curves of dominant PL peak change from reversed V shape to regular S shape when the excitation power increases. Additionally, a poorer thermal stability of sample B at high excitation power was found. These anomalous phenomena imply that there are two kinds of localized states of sample B which are induced by the relatively inhomogeneous indium distribution. These conclusions give us a further understanding of photoluminescence mechanism of green InGaN/GaN quantum wells and inhomogeneity effect at high excitation level which may help us in the manufacturing of InGaN/GaN laser diodes.

Abbreviations
HRXRD: High-resolution X-ray diffraction; LDs: Laser diodes; LEDs: Light-emitting diodes; LSE: Localized state ensemble; MOCVD: Metal-organic chemical vapor deposition system; MQWs: Multi-quantum wells; NH_3: Ammonia; PDPL: Power-dependent photoluminescence; RSM: Reciprocal space mapping; TDPL: Temperature-dependent photoluminescence; TMGa: Trimethylgallium; TMIn: Trimethylindium

Availability of Data and Materials
All data are fully available without restriction.

Authors' Contributions
The experiments and characterization presented in this work were carried out by YX and DGZ. All authors read and approved the final manuscript.

Authors' Information
Not applicable.

Competing Interests
The authors declare that they have no competing interests.

Publisher's Note
Springer Nature remains neutral with regard to jurisdictional claims in published maps and institutional affiliations.

Author details
[1]State Key Laboratory of Integrated Optoelectronics, Institute of Semiconductors, Chinese Academy of Science, Beijing 100083, China. [2]College of Materials Science and Opto-Electronic Technology, University of Chinese Academy of Sciences, Beijing 100049, China. [3]Center of Materials Science and Optoelectronics Engineering, University of Chinese Academy of Sciences, Beijing 100049, China. [4]Suzhou Institute of Nano-tech and Nano-bionics, Chinese Academy of Sciences, Suzhou 215123, China.

References
1. Fujita S (2015) Wide-bandgap semiconductor materials: for their full bloom. Jpn J Appl Phys 54:030101
2. Hardy MT, Feezell DF, Denbaars SP, Nakamura S (2011) Group III-nitride lasers: a materials perspective. Mater Today 14:408–415
3. Nakamura S (1999) InGaN-based violet laser diodes. Semicond Sci Technol 14:R27–R40
4. Zhao DG, J. Yang, Z. S. Liu, P. Chen, J. J. Zhu, D. S. Jiang, Y. S. Shi, H. Wang, L. H. Duan, L. Q. Zhang, and H. Yang (2017) Fabrication of room temperature continuous-wave operation GaN-based ultraviolet laser diodes. J. Semicond 38(5):051001
5. Zhao DM and Zhao DG (2018) Analysis of the growth of GaN epitaxy on silicon. J. Semicond 39(3):033006
6. Qi CL, Huang Y, Zhan T, Wang QJ, Yi XY, Liu ZQ (2017) Fabrication and characteristics of excellent current spreading GaN-based LED by using transparent electrode-insulator-semiconductor structure. J. Semicond 38(8): 084005
7. Cheong MG, Suh E-K, Lee HJ (2001) High-quality $In_{0.3}Ga_{0.7}N$/GaN quantum well growth and their optical and structural properties. Semicond Sci Technol 16:783–788
8. Narukawa Y, Kawakami Y, Funato M, Fujita S, Nakamura S (1997) Role of self-formed InGaN quantum dots for exciton localization in the purple laser diode emitting at 420 nm. Appl Phys Lett 70:981–983
9. Cheng C, Lei Y, Liu ZQ, He M, Li Z, Yi XY, Wang JX, Li JM, Xiong DP (2018) Performance improvement of light-emitting diodes with double superlattices confinement layer. J. Semicond 39(11):114005
10. Jiang LR, Liu JP, Tian AQ, Cheng Y, Li ZC, Zhang LQ, Zhang SM, Li DY, Ikeda M, Yang H (2016) GaN-based green laser diodes. J. Semicond 37(11):111001
11. Hammersley S, Kappers MJ, Massabuau FC-P, Sahonta S-L, Dawson P, Oliver RA, Humphreys CJ (2015) Effects of quantum well growth temperature on the recombination efficiency of InGaN/GaN multiple quantum wells that emit in the green and blue spectral regions. Appl Phys Lett 107:132106
12. Yang T-J, Shivaraman R, Speck JS, Wu Y-R (2014) The influence of random indium alloy fluctuations in indium gallium nitride quantum wells on the device behavior. J Appl Phys 116:113104
13. Auf der Maur M, Pecchia A, Penazzi G, Rodrigues W, Di Carlo A (2016) Efficiency drop in green InGaN/GaN light emitting diodes: the role of random alloy fluctuations. Phys Rev Lett 116:027401
14. Karpov SY (2017) Carrier localization in InGaN by composition fluctuations: implication to the 'green gap'. Photonics Res 5:A7
15. Jones CM, Teng C-H, Yan Q, Ku P-C, Kioupakis E (2017) Impact of carrier localization on recombination in InGaN quantum wells and the efficiency of nitride light-emitting diodes: insights from theory and numerical simulations. Appl Phys Lett 111:113501
16. Shahmohammadi M, Liu W, Rossbach G, Lahourcade L, Dussaigne A, Bougerol C, Butte R, Grandjean N, Deveaud B, Jacopin G (2017) Enhancement of Auger recombination induced by carrier localization in InGaN/GaN quantum wells. Phys Rev B 95:125314

17. Wang ZL, Wang L, Xing YC, Yang D, Yu JD, Hao ZB, Sun CZ, Xiong B, Han YJ, Wang J, Li HT, Luo Y (2017) Consistency on two kinds of localized centers examined from temperature-dependent and time-resolved photoluminescence in InGaN/GaN multiple quantum wells. ACS Photonics 4:2078–2084

18. Su ZC, Ning JQ, Deng Z, Wang XH, Xu SJ, Wang RX, Lu SL, Dong JR, Yang H (2016) Transition of radiative recombination channels from delocalized states to localized states in a GaInP alloy with partial atomic ordering: a direct optical signature of Mott transition? Nanoscale 8:7113–7118

19. Lao XZ, Yang Z, Su ZC, Wang ZL, Ye HG, Wang MQ, Yao X, Xu SJ (2018) Luminescence and thermal behaviors of free and trapped excitons in cesium lead halide perovskite nanosheets. Nanoscale 10:9949–9956

20. Su ZC, Xu SJ, Wang RX, Ning JQ, Dong JR, Lu SL, Yang H (2017) Electroluminescence probe of internal processes of carriers in GaInP single junction solar cell. Sol Energ Mat Sol C 168:201–206

21. Bao W, Su ZC, Zheng CC, Ning JQ, Xu SJ (2016) Carrier localization effects in InGaN/GaN multiple-quantum-wells LED nanowires: luminescence quantum efficiency improvement and "negative" thermal activation energy. Sci Rep 6:34545

22. Wang T, Parbrook PJ, Fan WH, Fox AM (2004) Optical investigation of InGaN/GaN multiple-quantum wells under high excitation. Appl Phys Lett 84:5159–5161

23. S. L. Rhode, W. Y. Fu, , M. A. Moram, F. C.-P. Massabuau, M. J. Kappers, C. McAleese, F. Oehler, C. J. Humphreys, R. O. Dusane, and S.–L. Sahonta, (2014) Structure and strain relaxation effects of defects in InxGa1−xN epilayers, J Appl Phys 116, 103513

24. Pozina G, Bergman JP, Monemar B, Takeuchi T, Amano H, Akasaki I (2000) Origin of multiple peak photoluminescence in InGaN/GaN multiple quantum wells. J Appl Phys 88:2677–2681

25. Yong-Hoon Cho GH, Gainer AJF, SongS JJ, Keller UKM, DenBaars SP (1998) S-shaped temperature-dependent emission shift and carrier dynamics in InGaN/GaN multiple quantum wells. Appl Phys Lett 73:1370–1372

26. Eliseev PG, Perlin P, Lee J, Osiński M (1997) Blue temperature-induced shift and band-tail emission in InGaN-based light sources. Appl Phys Lett 71:569–571

27. Wang HN, Ji ZW, Qu S, Wang G, Jiang YZ, Liu BL, Xu XG, Mino HF (2012) Influence of excitation power and temperature on photoluminescence in InGaN/GaN multiple quantum wells. Opt Express 20(4):3392–3940

28. Watson-Paris D, Godfrey MJ, Dawson P, Oliver RA, Galtrey MJ, Kappers MJ, Humphreys CJ (2011) Carrier localization mechanisms in In$_x$Ga$_{1-x}$N/GaN quantum wells. Phys Rev B 83:115321

29. Van Daele B, Van Tendeloo G, Jacobs K, Moerman I, Leys MR (2004) Formation of metallic in InGaN/GaN multiquantum wells. Appl Phys Lett 85:4379–4381

30. Hoffmann L, Bremers H, Jönen H, Rossow U, Schowalter M, Mehrtens T, Rosenauer A, Hangleiter A (2013) Atomic scale investigations of ultra-thin GaInN/GaN quantum wells with high indium content. Appl Phys Lett 102:102110

31. Liu JP, Wang YT, Yang H, Jiang DS, Jahn U, Ploog KH (2004) Investigations on V-defects in quaternary AlInGaN epilayers. Appl Phys Lett 84:5449–5451

32. Han D, Ma SF, Jia ZG, Jia W, Liu PZ, Dong HL, Shang L, Zhang AQ, Zhai GM, Li XM, Liu XG, Xu BS (2017) Photoluminescence close to V-shaped pits in the quantum wells and enhanced output power for InGaN light emitting diode. J Phys D Appl Phys 50:475103